

## Analysis of the Reaction $\pi^- + p \rightarrow \eta + n$ near Threshold\*

F. UCHIYAMA-CAMPBELL AND R. K. LOGAN

*Department of Physics, University of Illinois, Urbana, Illinois*

(Received 4 May 1966)

We successfully fit both the total and the differential cross sections for the reaction  $\pi^- + p \rightarrow \eta + n$  in the region of  $T_{\pi^-}$  from threshold (558 MeV) to 900 MeV with both multichannel Breit-Wigner and effective-range formulas. We find that an  $S$ -wave resonance accounts for the enhancement of the reaction near threshold. A comparison is made of the various  $\pi p$   $S_{11}$  phase-shift analyses with the phase shifts predicted by our multichannel fits. A search was made for the  $S$ -matrix poles of our Breit-Wigner and effective-range solutions on the various sheets of the energy plane.

THE measurement of the reaction  $\pi^- + p \rightarrow \eta + n$  by Bulos *et al.*<sup>1</sup> revealed an enhancement of the total  $\eta$  production cross section  $\sigma_{\eta}^T$  just above threshold. Several authors,<sup>2-5</sup> with varying degrees of success, have attempted to show that this enhancement is due to a pole of the  $S_{11}$  partial-wave scattering amplitude. A scattering-length-approximation fit<sup>2</sup> of both the reaction data and the  $\pi p$  elastic-scattering phase shifts failed to reveal evidence of a pole. A more successful multichannel effective-range approach was attempted by Hendry *et al.*<sup>3</sup> Although they could not find solutions by considering two channels (i.e., the  $\pi p$  and  $\eta n$  channels), they were able to find a resonance by considering more than two channels. They achieved a similar success using a Breit-Wigner form for the scattering amplitude instead of the effective-range approximation. The more recent measurements of Richards *et al.*<sup>6</sup> have reconfirmed the enhancement of  $\sigma_{\eta}^T$ . They have also revealed a nonisotropic angular distribution, however, which the older data<sup>1</sup> did not.

We shall analyze the more recent data, fitting both the total and differential cross sections. Because of the large disparities between the various phase-shift solutions,<sup>7-11</sup> we felt that fitting the reaction and elastic data simultaneously might prove misleading. We have therefore handled the reaction data independently of the phase-shift analyses. We were able to explain the

enhancement of  $\sigma_{\eta}^T$  in terms of a two-channel  $S$ -wave Breit-Wigner resonance. The angular distributions were fitted by adding small amounts of  $P$  and  $D$  wave to the dominant  $S$ -wave term. A successful two-channel effective-range fit to the data was also performed, yielding results similar to the Breit-Wigner fit.

The sharp rise of  $\sigma_{\eta}^T$  just above threshold indicates that  $\eta$  production is mainly  $S$  wave. This is verified by the fact that only an  $S$ -wave resonance fits  $\sigma_{\eta}^T$ . Additional supporting evidence for  $S$ -wave dominance may be obtained by considering the energy dependence of the  $S_{11}$   $\pi p$  inelasticity parameter  $\eta_S$ . For a majority of the phase-shift solutions,  $\eta_S$  is exactly one below the  $\eta n$  threshold. Above threshold  $\eta_S$  becomes less than one, reaching a minimum at the precise energy at which  $\sigma_{\eta}^T$  is a maximum. This demonstrates the dominance of the inelastic part of  $S_{11}$  by  $\eta$  production. This agrees with the results of Yodh,<sup>12</sup> which showed that the  $T = \frac{1}{2}$  one-pion production (the only other  $\pi p$  reaction at this energy with a non-negligible cross section) is principally  $P$  and  $D$  wave. One can estimate the relative contribution of the  $S_{11}$  wave to  $\sigma_{\eta}^T$  by comparing the experimental values of  $\sigma_{\eta}^T$  with the values of<sup>13</sup>  $(2/9)(\pi/q_1^2)(1-\eta_S^2)$  obtained from the various phase-shift solutions ( $q_1$  is c.m. momentum of the  $\pi p$  system). This comparison reveals that  $\eta$  production is almost entirely  $S$  wave. This dominance is not complete, however, because of the nonisotropy of the angular distribution. There must be small contributions from other waves. In fact, Richards *et al.*<sup>6</sup> have shown with a Legendre polynomial fit of the differential cross section that there are  $P_1(\cos\theta)$  and  $P_2(\cos\theta)$  terms. These terms are most easily accounted for by assuming that the  $S_{11}$  waves interfere with small contributions from the  $P_{11}$  and  $D_{13}$  waves.

Our model for fitting the reaction data consists of contributions from the three partial waves:  $S_{11}$ ,  $P_{11}$ , and  $D_{13}$ .<sup>14</sup> The  $S$ -wave is assumed to be dominated by a two-channel resonance. With the  $K$  matrix defined by  $S = (1+iK)(1-iK)^{-1}$ , the  $S$ -wave elements of  $K$  are

\* Work supported by the U. S. Office of Naval Research under Contract No. Nonr 1834(05).

<sup>1</sup> F. Bulos, R. E. Lanon, A. E. Pifer, A. M. Shapiro, M. Widgoff, R. Panvini, A. E. Brenner, C. A. Bordner, M. E. Law, E. E. Ronat, K. Stranch, J. J. Szymanski, P. Bastien, B. B. Brabson, Y. Eisenberg, B. T. Feld, V. K. Fisher, I. A. Pless, L. Rosenson, R. K. Yamamoto, G. Cavelli, L. Guerriero, G. A. Salandin, A. Tomasin, L. Ventura, C. Voci, and F. Waldner, *Phys. Rev. Letters* **13**, 486 (1964).

<sup>2</sup> F. Uchiyama-Campbell, *Phys. Letters* **18**, 189 (1965).

<sup>3</sup> A. W. Hendry and R. G. Moorhouse, *Phys. Letters* **18**, 171 (1965).

<sup>4</sup> J. S. Ball, *Phys. Rev.* **149**, 1191 (1966).

<sup>5</sup> S. C. Michael, *Phys. Letters* **21**, 93 (1966).

<sup>6</sup> W. B. Richards *et al.*, *Phys. Rev. Letters* **16**, 1221 (1966).

<sup>7</sup> B. H. Bransden, P. J. O'Donnell, and R. G. Moorhouse, *Phys. Rev.* **139**, 1566 (1965).

<sup>8</sup> P. Bareyre, C. Brickman, A. V. Stirling, and G. Villet, *Phys. Letters* **18**, 342 (1965).

<sup>9</sup> P. Auvil, C. Lovelace, A. Donnachie, and A. T. Lea, *Phys. Letters* **12**, 76 (1964).

<sup>10</sup> J. Cence, *Phys. Letters* **20**, 306 (1966).

<sup>11</sup> L. D. Roper, R. M. Wright, and B. T. Feld, *Phys. Rev.* **138**, 190 (1965).

<sup>12</sup> G. B. Yodh, University of Maryland, Technical Report No. 512, 1966 (unpublished).

<sup>13</sup> The factor of  $2/9$  arises from a  $\frac{2}{3}$  coming from isospin consideration and a  $\frac{1}{3}$  from the branching ratio of  $\eta \rightarrow 2\gamma$ .

<sup>14</sup> From here on we shall drop the subscripts and denote these waves by  $S$ ,  $P$ , and  $D$ , respectively.

TABLE I. The parameters and  $\chi^2$  for the Breit-Wigner solutions.

Solution	$w_S$ (MeV)	$\Gamma(w_S)$ (MeV)	$g_1$	$\Gamma_1(w_S)$ (MeV)	$g_2$	$\Gamma_2(w_S)$ (MeV)	$C_P$ (BeV <sup>-4</sup> )	$(\Gamma_1\Gamma_2)_P$ (MeV <sup>2</sup> )	$C_D$ (BeV <sup>-8</sup> )	$(\Gamma_1\Gamma_2)_D$ (MeV <sup>2</sup> )	$\chi^2$
BW-I	1557	156	0.23	110	0.207	46	0.61	90	3.03	16	33.7
BW-II	1565	144	0.085	41	0.44	103	0.61	90	3.03	16	31.1

chosen to be

$$K_{ij}^S = \frac{1}{2}(\Gamma_i\Gamma_j)^{1/2}/(w-w_S), \quad (1)$$

where  $i$  and  $j$  run over 1 and 2 and represent the  $\pi p$  and  $\eta n$  channels, respectively,  $w$  is the center-of-mass total energy, and  $w_S$  is the position of the resonance. The quantities  $\Gamma_1$  and  $\Gamma_2$  are related to the center-of-mass momentum  $q_1$  and  $q_2$  of these channels by the equation  $\Gamma_j = g_j q_j$ , where  $g_1$  and  $g_2$  are constants. The partial-wave scattering amplitude from channel  $i$  to channel  $j$ ,  $f_{ij}^S$ , is related to  $K_{ij}^S$  by

$$f_{ij}^S = K_{ik}(1 - iK)_{kj}^{-1}. \quad (2)$$

Substituting Eq. (1) into Eq. (2) we have

$$f_{ij}^S = \frac{\frac{1}{2}(\Gamma_i\Gamma_j)^{1/2}}{w_S - w - \frac{1}{2}i(\Gamma_1 + \Gamma_2)} \equiv \frac{N_{ij}}{D}. \quad (3)$$

These amplitudes may be expressed in terms of  $\eta_S$  and the real part of the elastic phase shift  $\delta_1^S$  by

$$f_{jj}^S = \frac{\eta_S e^{2i\delta_j^S} - 1}{2i} \quad (4)$$

and

$$f_{12}^S = \frac{1}{2}(1 - \eta_S^2)^{1/2} e^{i(\delta_1^S + \delta_2^S)}. \quad (5)$$

We shall assume that the  $P_{11}$  and  $D_{13}$   $\pi p$  resonances couple to the  $\eta n$  channel, as well as the  $\pi p$  and the other inelastic channels. The partial-wave scattering amplitude for these two waves is thus given by

$$f_{12}^l = \frac{\frac{1}{2}(\Gamma_{1l}\Gamma_{2l})^{1/2}}{w_l - w - \frac{1}{2}(i)\Gamma_l} \quad l = P, D, \quad (6)$$

where the total width  $\Gamma_l > \Gamma_{1l} + \Gamma_{2l}$ . The values of  $w_l$  and  $\Gamma_l$  can be derived from the phase-shift analyses of the  $\pi p$  system. The products  $\Gamma_{1l}\Gamma_{2l} = C_l q_1^{2l+1} q_2^{2l+1}$  are unknowns, however. Our model therefore contains five parameters  $w_S$ ,  $g_1$ ,  $g_2$ ,  $C_P$ , and  $C_D$  which may be varied. There is very little ambiguity in determining the values  $w_D = 1531$  MeV and  $\Gamma_D = 120$  MeV from the various phase-shift solutions.<sup>7-11</sup> Determining the parameters of the  $P_{11}$  wave is a great deal more difficult; indeed, there is disagreement among the various solutions as to whether or not  $P_{11}$  is resonant. We choose the values  $w_P = 1503$  MeV and  $\Gamma_P = 308$  MeV. As we shall see later, our results do not depend crucially on this choice.

We have fitted the six total-cross-section data points of Ref. 1 below  $T_\pi = 900$  MeV ( $T_\pi$  equals the pion

kinetic energy in the lab) along with four total cross-section and 40 differential cross-section points of Ref. 6 at  $T_\pi = 592, 655, 704,$  and  $875$  MeV. Four of the total cross-section points were used to normalize the four angular distributions; hence there are 46 independent data points. Our fit therefore has 41 degrees of freedom, since there are five free parameters. Our least-squares fit revealed two regions of our parameter space where  $\chi^2$  was less than 41. The local minima of these two regions are listed in Table I. The fits<sup>15</sup> to the data are displayed in Fig. 1. The observed cross sections<sup>1,6</sup> shown there are about  $\frac{1}{3}$  of the true  $\eta$  production cross sections because only those  $\eta$ 's which decayed into  $2\gamma$  were observed and the branching ratio for this mode is approximately  $\frac{1}{3}$ . Although the exact value of the branching ratio is uncertain, it does lie somewhere

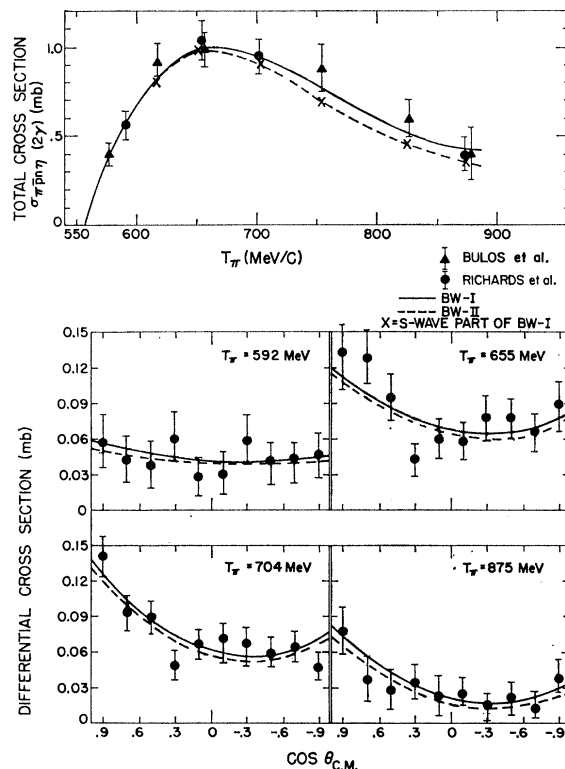


FIG. 1. The fit of the two Breit-Wigner solutions of the experimental total and differential  $\eta$  production cross sections.

<sup>15</sup> Note that the experimental angular distributions are not the true  $\eta$  angular distributions, but the  $\eta$  bisector distributions (i.e., the distribution of the bisector of the two  $\gamma$  rays coming from the decay  $\eta \rightarrow 2\gamma$ ). The difference between these two distributions, however, is considerably less than the experimental errors.

TABLE II. The location of the poles of both the Breit-Wigner and effective-range scattering amplitudes on the four sheets of the energy plane in terms of the real and imaginary part of  $w$ . No poles were found on sheet I.

Sheet \ Solution	BW-I (MeV)	BW-II (MeV)	E-I (MeV)	E-II (MeV)	E-III (MeV)	E-IV (MeV)
II	Rew Imw 1560 ±32	No pole	1575 ±31	No pole	No pole	No pole
III	Rew Imw 1537 ±76	1540 ±70	1547 ±90	1546 ±73	1535 ±154	1582 ±83
IV	Rew Imw No pole	1555 ±27	No pole	1564 ±15	1567 ±35	1579 ±22

between 0.38 and 0.31.<sup>4</sup> The results of our analysis, however, do not depend sensitively on this value. This is because a change of the branching ratio changes the over-all normalization of  $\sigma_{\eta}^T$ , which can be accounted for by changing  $g_1$  and  $g_2$  by a few percent. The contribution of the  $S$  wave alone to  $\sigma_{\eta}^T$  is shown for one of the solutions to show the dominance of this wave over  $P$  and  $D$ . Because of the ambiguity in determining the values  $w_P$  and  $\Gamma_P$ , we also checked the sensitivity of our results to these values. We found that our results were very insensitive to either the magnitude or energy dependence of  $w_P$  and  $\Gamma_P(w)$ , and hence that our results are independent of our model for the  $P$  wave.

The two solutions we found correspond to resonances at 1557 and 1565 MeV with full widths,  $\Gamma(w_S)$ , of 156 and 144 MeV, respectively. The major difference

between the two solutions, however, is the fact that for solution BW-I  $g_1 \approx g_2$  [or  $\Gamma_1(w_S) > \Gamma_2(w_S)$ ], whereas for solution BW-II  $g_2 \gg g_1$  [or  $\Gamma_1(w_S) < \Gamma_2(w_S)$ ]. This leads to differences in the behavior of the elastic phase shifts. The values of  $\delta_1$  and  $\delta_2$  for both solutions were obtained with the help of Eqs. (3) and (4). All our phase shifts have a cusp at the  $\eta n$  threshold. The values of  $\delta_1$  are plotted in Fig. 2. Note that  $\delta_1(w_S)$  goes through  $90^\circ$  for solution BW-I and through  $0^\circ$  for solution BW-II. We found the opposite behavior for  $\delta_2(w)$ , i.e.,  $\delta_2(w_S) = 0^\circ$  for BW-I and  $90^\circ$  for BW-II. Comparison of  $\delta_1(w)$  with the various phase shift solutions<sup>7-11</sup> shows that solution BW-I most resembles Bransden's I,<sup>7</sup> while solution BW-II is somewhat like Bransden's II<sup>7</sup> or Auvil's.<sup>9</sup> The disparity between the various phase-shift solutions<sup>7-11</sup> is greatest above  $T_\pi = 600$  MeV. Below this energy they more or less agree. Note that BW-I gives somewhat better agreement with these values below 600 than BW-II.

The positions of the poles of solutions BW-I and BW-II are found by searching the four sheets of the complex  $w$  plane near the second threshold for the zeros of the complex denominator  $D$  of Eq. (3). In denoting these four sheets we shall use the notation of Frazer and Hendry.<sup>16,17</sup> Sheet I, or the physical sheet, has two cuts along the positive real axis beginning at the  $\pi p$  and  $\eta n$  thresholds, respectively. The unphysical sheets II and III, are connected directly to the real axis (between the two thresholds for sheet II and above the  $\eta n$  threshold for sheet III). Sheet IV, the super-unphysical sheet, on the other hand, is not directly connected to the physical axis except at the point  $w_{TH}$ , the energy of the  $\eta n$  threshold. For each of our solutions we find two pairs of poles, one of which is on sheet III near the real axis, just above the  $\eta n$  threshold. The other pair of poles is on sheet II for solution BW-I and sheet IV for BW-II. The exact location of the poles are listed in Table II. The dependence of the location of the poles on  $g_1$  and  $g_2$  is

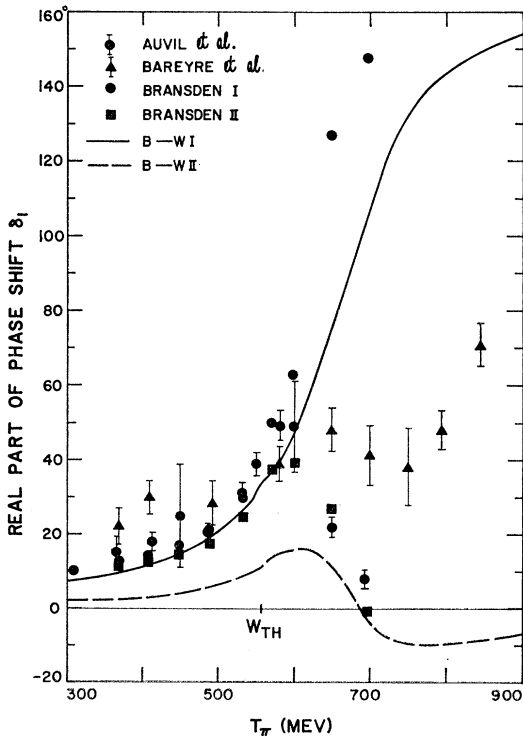


FIG. 2. A plot of  $\delta_1$  versus  $T_\pi$  for the four phase-shift solutions of Refs. 6-8 and the two Breit-Wigner solutions BW-I and BW-II.

<sup>16</sup> W. R. Frazer and A. W. Hendry, Phys. Rev. 134, B1307 (1964).

<sup>17</sup> The sheet structure of the  $w$  plane near the  $\eta n$  threshold for the Breit-Wigner scattering amplitude and the effective-range amplitude happens to be the same as that of the  $s$  plane discussed in Ref. 13. The definition of  $\theta_1$  and  $\theta_2$  for the  $w$  plane is completely analogous. We shall number the sheets of the  $w$  plane just as Frazer and Hendry numbered the sheets of the  $s$  plane.

TABLE III. The parameters,  $\chi^2$ , and phase shifts for the effective-range solutions.

Solution	$M_{11}$ (BeV)	$M_{22}$ (BeV)	$M_{12}$ (BeV)	$R_1$	$R_2$	$C_P$ (BeV <sup>-4</sup> )	$C_D$ (BeV <sup>-8</sup> )	$\chi^2$	$\delta_1(T_\pi=680)$ MeV	$\delta_2(T_\pi=680)$ MeV
I	-28.0	-28.0	-28.34	-4.0	-4.0	0.44	2.21	44.1	80°	4°
II	-28.0	-8.4	-15.73	-4.0	-4.0	0.44	2.48	44.4	0°	73°
III	0.25	0.35	0.51	-4.5	4.5	1.0	3.31	44.4	6°	5°
IV	-0.56	0.14	0.59	-4.0	-4.0	0.61	2.21	49.0	174°	47°

similar to a Breit-Wigner model discussed by Eden and Taylor.<sup>18</sup>

Although the results of our Breit-Wigner analysis does not provide a clear choice for  $\delta_1$ , it does favor solutions which go through either 0° or 90° near  $T_\pi=680$  MeV. This might be due to our use of the Breit-Wigner form to fit the reaction data rather than the uniqueness of our fits. To test whether or not this is the case, we have attempted fitting the data with a model in which  $f_{ij}^s$  is given by an effective-range approximation. The  $P$  and  $D$  waves are treated just as before. The inverse of  $K^s$ , however, is expanded about the  $\eta n$  threshold in powers of  $(w-w_{TH})$ , viz.,

$$K_{ij}^{-1}(w) = M_{ij} + (w-w_{TH})R_{ij}\delta_{ij}, \quad (7)$$

where  $M_{ij}$  and  $R_{ij}$  are constants and  $w_{TH} = M_P + M_\eta = 1488$  MeV [ $(T_\pi)_{TH} = 557$  MeV]. Ross and Shaw<sup>19</sup> have shown that to a good approximation  $R_{ij}$  may be taken diagonal. Our expression for  $f_{ij}^s$  is obtained by substituting Eq. (7) into Eq. (2), from which we obtain

$$f_{12}^s = \frac{M_{12}}{(A_1A_2 - q_1q_2 - M_{12}^2) - i(q_1A_2 + q_2A_1)} = \frac{M_{12}}{D_{EFF}}, \quad (8)$$

where  $A_i = M_{ii} + R_{ii}(w-w_{TH})$ . With this model we have seven free parameters altogether,  $M_{11}$ ,  $M_{22}$ ,  $M_{12}$ ,  $R_1$ ,  $R_2$ ,  $C_P$ , and  $C_D$ . We found four regions of our parameter space for which  $\chi^2$  was small. These four solutions, along with their respective  $\chi^2$ , are listed in Table III. The phase shifts for each of our four effective-range solutions were calculated using Eqs. (2), (4), and (7). Plots of  $\delta_1$  versus  $T_\pi$  for the four different solutions are shown in Fig. 3 and the values of  $\delta_1$  and  $\delta_2$  at  $T_\pi=680$  MeV are listed in Table III. We see that the phase shifts of solutions E-I and E-II behave almost exactly like those of solutions BW-I and II, respectively.  $\delta_1$  for E-III is similar to BW-II, but  $\delta_2$  is quite different. As mentioned before, the various phase-shift solutions<sup>7-11</sup> agree below  $T_\pi=600$  MeV. Of our four effective-range solutions, only the phase shifts for E-I agree with these values. Those of E-II and E-III are similar in shape but too small in magnitude, while those of E-IV differ drastically. Therefore, shall not consider E-IV a solution.

The poles of the effective-range solutions were found by searching the  $w$  plane, as before, for the zeros of the

denominator  $D_{EFF}$  of Eq. (8). Two pairs of poles were found for each of the solutions. They are listed in Table II. Note that the poles of E-I and E-II are at almost the same positions of the poles belonging to the BW solutions I and II, respectively. Since the behavior of  $\delta_1(w)$  and  $\delta_2(w)$  and the location of their poles is identical, it may safely be assumed that E-I and E-II are the effective-range approximations of BW-I and II, respectively.

The results of our effective-range fits are very encouraging. First of all, they yield the two BW solutions we obtained earlier. Secondly, although there is another solution (E-III), they all share the common feature that  $\delta_1$  is approximately 0° or 90° at  $T_\pi=680$  MeV. The phase shifts for the effective-range approximation,

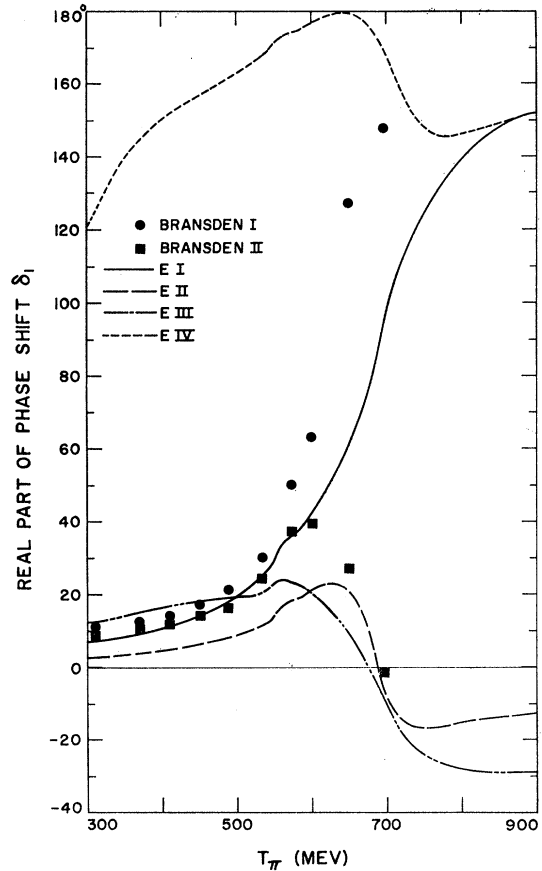


FIG. 3. A plot of  $\delta_1$  versus  $T_\pi$  for the two phase-shift solutions of Ref. 7 and the four effective-range solutions E-I-IV.

<sup>18</sup> R. J. Eden and J. G. Taylor, Phys. Rev. Letters 11, 516 (1963).

<sup>19</sup> M. H. Ross and G. L. Shaw, Ann. Phys. (N.Y.) 13, 147 (1961).

however, are not constrained to go through  $0^\circ$  or  $90^\circ$  like the BW phase shifts. Another common feature of all our BW and effective-range fits of the reaction data is that each has a pole on sheet III near the real axis 50 to 60 MeV above threshold. This is a good indication that the enhancement of  $\sigma_{\gamma}^T$  is a resonance phenomenon.<sup>20</sup>

<sup>20</sup> We note, however, that in the present circumstances the resonance is caused by poles on both sheet III and sheet II (or IV).

It is a pleasure for us to thank Professor J. D. Jackson for his frequent and valuable discussions. We also wish to thank Professor K. Dietz and Professor R. Schult for their helpful comments. One of us (F. U.-C.) wishes to thank Professor G. M. Almy for his hospitality.

Only when the poles lie far from threshold (in units of  $\Gamma$ ) does the pole on sheet III dominate the resonance.

## Connection between the Electromagnetic Form Factor and the Propagator Normalizations\*†

ROBERT G. CAWLEY

Clarkson College of Technology, Potsdam, New York

(Received 15 April 1966)

The Ward identity is used to display the connection between the electromagnetic form factor and propagator normalizations.

### I. INTRODUCTION

IN the context of asymptotic field theory the normalization of the propagator for the interpolating fields comes from the normalization of the asymptotic fields and spectrum, as is well-known.<sup>1</sup> Within the context of such a theory it is possible to introduce electromagnetic interactions, without recourse to a Lagrangian, by adopting the Ward-Takahashi equations as supplementary conditions characterizing quantum electrodynamics.<sup>2</sup> The particle electromagnetic form factors of the theory are then defined as matrix elements of the electromagnetic current between single-particle states. The customary procedure in fixing the normalizations of these form factors is to require the space integral of their zero-momentum-transfer values to be equal to the observed particle charge. It is possible however to show that the normalization of these form factors follows from just the propagator normalization and the Ward-Takahashi equations. It is the purpose of this paper to show this.

One difficulty we do not deal with is that of the *existence* of the asymptotic condition in the presence of the electromagnetic interactions. The difficulty alluded to here is that associated with the zero mass of the photon. In this connection we will find it necessary to postulate the normalization of the photon propagator.

\* Supported by the U. S. Office of Naval Research.

† This work is based on a part of the author's Ph.D. thesis at the University of Illinois.

<sup>1</sup> See, for example, the derivation of the Källén-Lehmann representation for the propagator in G. Barton, *Introduction to Advanced Field Theory* (Interscience Publishers, Inc., New York, 1963), p. 50ff.

<sup>2</sup> K. Nishijima, *Phys. Rev.* **119**, 485 (1960).

We demonstrate the connection between the normalization conditions for scalar and vector fields by way of example. Section II reviews the derivation of the Ward identity (which is all we need for our proof) from the Ward-Takahashi equations. Section III, in the well-known way, relates the electromagnetic form factor to the vertex function arising out of the Ward identity, the (unit) normalization of the particle propagator being carried along for didactic reasons. Section IV discusses the propagator and its tensor properties, and Sec. V completes the derivation of the equality of the two normalization conditions by assembling the results of the preceding sections.

### II. DERIVATION OF THE WARD IDENTITY

The Feynman propagator of a complex scalar field  $\Phi(x)$  is

$$\Delta_{F'}(x_1-x_2) = \langle 0 | T[\Phi(x_1)\Phi^\dagger(x_2)] | 0 \rangle, \quad (\text{II.1})$$

where  $\Phi(x)$  is the particle-interpolating field operator. The momentum-space propagator is defined by

$$\Delta_{F'}(x_1-x_2) = \frac{-i}{(2\pi)^4} \int d^4p e^{ip \cdot (x_1-x_2)} \Delta_{F'}(p), \quad (\text{II.2})$$

where we use the Minkowski (space-favored) metric  $p \cdot x = \mathbf{p} \cdot \mathbf{x} + p_4 x_4 = \mathbf{p} \cdot \mathbf{x} - p_0 x_0$ .

The electromagnetic (vector photon) vertex function is defined by

$$\begin{aligned} \langle 0 | T[\Phi(x_1)\Phi^\dagger(x_2)A_\lambda(x_3)] | 0 \rangle = & -q \int d^4x_1' \int d^4x_2' \int d^4x_3' \\ & \times \Delta_{F'}(x_1-x_1') \Gamma_{\lambda'}(x_1'-x_3'; x_3'-x_2') \Delta_{F'}(x_2'-x_2) \\ & \times D_{F'\lambda'\lambda}(x_3'-x_3), \quad (\text{II.3}) \end{aligned}$$